Available online at www.sciencedirect.com
ScienceDirect
Journal of Nuclear Materials 363–365 (2007) 1044–1049
journal of nuclear materials
www.elsevier.com/locate/jnucmat

Modeling of dynamic response of SOL-divertor plasmas to an ELM crash

N. Hayashi [a,*], T. Takizuka [a], M. Hosokawa [b]

[a] Japan Atomic Energy Agency, 801-1 Mukouayama, Naka, Ibaraki 311-0193, Japan
[b] Research Organization for Information Science and Technology, Tokai, Ibaraki 319-1106, Japan

Abstract

A dynamic five-point model is developed to study responses of scrape-off-layer (SOL) and divertor plasmas to a crash due to edge-localized modes (ELMs). The five-point model is beneficial to wide-ranging studies of SOL-divertor physics and to coupling with the core transport code in the integrated modeling. The five-point model can reproduce static and dynamic features obtained by usual fluid codes. The dynamic behavior obtained by the five-point model agrees fairly well with that by the particle code PARASOL. The influence of the ELM crash on the thermoelectric instability and the resultant asymmetry is investigated. The ELM crash transiently induces the thermoelectric instability and large SOL currents for asymmetric divertor plasmas before the ELM. The resultant currents drive convective heat flows and enhance the asymmetry on the fast time scale of electrons. The ELM crash is found to reverse the asymmetry before and after the ELM. Even for symmetric plasmas before the ELM, the asymmetry is induced on the slow time scale of ions by an ELM crash, because the transient formation of dense and cold divertor plasmas causes the thermoelectric instability.

PACS: 52.35.Py; 52.55.Fa; 52.65.−y; 52.65.Kj

Keywords: Divertor modeling; Divertor asymmetry; SOL current; ELM; Thermoelectric instability

1. Introduction

Transient heat and particle fluxes to the divertor plates caused by edge-localized modes (ELMs) are crucial in terms of damage and lifetime of the divertor plates in tokamak reactor operations. Understanding the dynamic behavior of the scrape-off-layer (SOL) and divertor plasmas after an ELM crash is then important for fusion research.

Enhanced heat and particle fluxes due to ELMs have been experimentally investigated in divertor tokamaks [1,2]. Additionally, in/out or up/down asymmetry of the enhanced heat flux by ELMs between the two plates at both ends of an open magnetic field line has been observed in experiments [2] and 2-dimensional fluid simulations [3]. While 2D fluid simulations consume much calculation-time, a two-point model based on integral fluid equations easily reproduces many static features found in experiments [4]. Such point models are suitable not only for studying physics in a wide range of

* Corresponding author. Fax: +81 29 270 7419.
E-mail address: hayashi.nobuhiko@jaea.go.jp (N. Hayashi).

0022-3115/$ - see front matter
doi:10.1016/j.jnucmat.2007.01.159

parameter space but also for coupling with core transport codes [5]. The edge boundary conditions at the separatrix were also found to affect the ELM behavior in the simulation with a transport code including an ELM model [6]. A dynamic version of the point model is necessary for the study of the dynamic nature of SOL-divertor plasmas after ELMs and is beneficial to the integrated ELM modeling.

In addition, the two-point model cannot deal with the asymmetry. A five-point model was successful in clarifying static features of the asymmetry caused by the thermoelectric instability [7,8]. The SOL current driven by the thermoelectric sheath potential causes this instability and increases the temperature asymmetry by driving a convective electron heat toward the hotter divertor plasma. For the high-temperature SOL plasma just after an ELM, the instability may arise and a large heat flux may concentrate on a single-side plate.

In this paper, we develop a dynamic five-point model and investigate the dynamic responses of the SOL-divertor plasmas to an ELM crash. The dynamic five-point model introduces kinetic-effect on the basis of results from the particle simulation code PARASOL [9]. The results of the five-point model are then compared with results of usual fluid codes and PARASOL. The influence of ELM on the thermoelectric instability and the asymmetry is also examined.

2. Dynamic five-point model

The model is based on time dependent fluid equations, i.e., particle, momentum, electron and ion energies, generalized Ohm's law and current equations. Currents perpendicular to the magnetic field and the momentum loss are not taken into account at present for simplicity. The previous model in Refs. [7,8] treated the stationary phase $\partial/\partial t = 0$ with $T_e = T_i$ assuming that the ion heat conduction can be neglected.

Fig. 1 shows a geometry of the model. We consider an open magnetic flux tube nearest to the separatrix in single-null or double-null plasmas. The flux tube is divided into four regions. The SOL region, with a length along the magnetic field L_{SOL}, is divided into two regions with lengths l_a and l_b ($L_{SOL} = l_a + l_b$) on either side of the stagnation point where the parallel particle flux is zero. The two divertor regions are assumed to have the same length, L_{div}, in this paper.

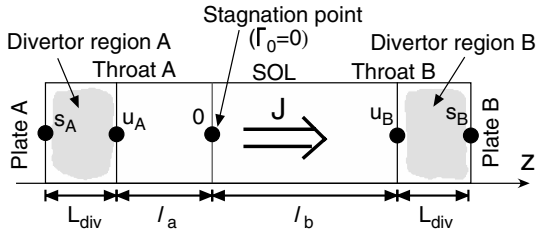

Fig. 1. Geometry of five-point model where z denotes length along magnetic field line.

The equations are integrated along the magnetic field in each region. The momentum equation is integrated from the stagnation point to the divertor plate. The resultant equations of density, n, ion particle flux, Γ, electron and ion temperatures, T_e, T_i, are given as

$$L_{SOL}\mathrm{d}n_0/\mathrm{d}t = -\Gamma_{uB} - \Gamma_{uA} + S_0 L_{SOL}, \quad (1)$$

$$L_{div}\mathrm{d}n_{sA,B}/\mathrm{d}t = \Gamma_{uA,B} - \Gamma_{sA,B} + S_{A,B}L_{div}, \quad (2)$$

$$0.5m_i(l_{a,b} + (R_{A,B}+1)L_{div})\,\mathrm{d}\Gamma_{uA,B}/\mathrm{d}t = n_0(T_{e0}+T_{i0}) - n_{sA,B}(2T_{esA,B} + (1+g)T_{isA,B}), \quad (3)$$

$$1.5L_{SOL}\mathrm{d}(n_0T_{j0})/\mathrm{d}t = -Q_{juB} - Q_{juA} - \delta_j J(\phi_{uB} - \phi_{uA}) + (W_{j0} + W_{jeq0})L_{SOL}, \quad (4)$$

$$1.5L_{div}\mathrm{d}(n_{sA,B}T_{jsA,B})/\mathrm{d}t = Q_{juA,B} - Q_{jsA,B} + \delta_j\sigma_{A,B}J(\phi_{uA,B} - \phi_{sA,B}) + (W_{jA,B} + W_{jeqA,B})L_{div}, \quad (5)$$

where subscripts, 0, u, and s, denote the stagnation point, the upstream throat of the divertor region, and the sheath entrance, respectively. The subscripts, A and B, indicate the two divertor regions on either side of the SOL. In Eqs. (4) and (5), a subscript, j, denotes particle species, electrons or ions, and $\delta_e = 1$, $\delta_i = 0$, and $\sigma_A = -1$, $\sigma_B = 1$. The particle and energy sources in the SOL region, S_0, W_{j0}, are due to the radial diffusion from the core into the SOL and are functions of radial particle and heat fluxes, Γ_r and Q_{jr}, and diffusivities, $D_\perp$ and $\chi_{j\perp}$ (see Ref. [7] with the separation of T_e and T_i). The values of Γ_r and Q_{jr} are assumed to be uniform on the last closed flux surface and net radial fluxes, Φ_{sep} and Q_{jsep}, as well as $D_\perp$ and $\chi_{j\perp}$ are inputs of the model. In the divertor region, recycling and impurity radiation are assumed to be given by $S_{A,B} = \eta_r\Gamma_{sA,B}/L_{div}$, $W_{eA,B} = -k\cdot\Delta E\cdot S_{A,B}$ and $W_{iA,B} = 0$, where η_r denotes the recycling coefficient, k denotes the effective radiation factor, and $\Delta E = 13.6$ eV. In Eq. (3), the particle flux amplification factor is defined by $R_{A,B} = \Gamma_{sA,B}/\Gamma_{uA,B}$. The upstream heat flux including both conductive and convective fluxes is given by,

$$Q_{j\mathrm{uA,B}} = Q_{j\mathrm{eff}} - \delta_j \sigma_{\mathrm{A,B}} \left(\frac{5}{2} + \alpha\right) T_{\mathrm{euA,B}} \frac{J}{e} + \frac{5}{2} T_{j\mathrm{uA,B}} \Gamma_{\mathrm{uA,B}}, \quad (6)$$

where the first term on RHS is the effective conductive flux with the flux limit, $Q_{j\mathrm{eff}} = (Q_{j\mathrm{cl}}^{-h} + Q_{j\mathrm{lim}}^{-h})^{-1/h}$, $Q_{j\mathrm{cl}} = (2/7)\kappa_{j^*}(T_{j\mathrm{uA,B}}^{3.5} - T_{j\mathrm{sA,B}}^{3.5})/L_{\mathrm{div}}$, $Q_{j\mathrm{lim}} = \alpha_j n_0 T_{j\mathrm{uA,B}}^{1.5}/m_j$, and $\kappa_{j^*} = \kappa_{j\|}/T_j^{2.5}$. For the values of h and α_j, a heat-flux-limit model obtained from PARASOL [9] is used, yielding $h = 4/3$ and $\alpha_e = 3/4$ for electrons. The same model is assumed for ions; $\alpha_i = 3/4$. Another model with $h = 1$ and $\alpha_j = 1.5$ [10] does not change the results much. The value of $\alpha = 0.71$ mean the thermal force coefficient. The upstream temperature, $T_{j\mathrm{uA,B}}$, is defined in the same way as in Ref. [8] except for the separation of T_e and T_i. The SOL current density, J, is derived from the sum of integrated equations of Ohm's law and sheath potentials,

$$-\bar{\eta} L_{\mathrm{SOL}} J = \sum_{d=\mathrm{A,B}} \sigma_{\mathrm{d}} \left(\beta_{\mathrm{d}} - \alpha + n_0 T_{\mathrm{e0}}/(n_{\mathrm{sd}} T_{\mathrm{esd}}) - 1 - \ln\left(1 - \sigma_{\mathrm{d}} \widehat{J}_{\mathrm{d}}\right)\right) T_{\mathrm{esd}}/e, \quad (7)$$

where $\beta_{\mathrm{A,B}} = 0.5\ln(m_i/(2\pi m_e))(T_{\mathrm{esA,B}}/(T_{\mathrm{esA,B}} + gT_{\mathrm{isA,B}}))$, $\widehat{J}_{\mathrm{A,B}} = J/\Gamma_{\mathrm{sA,B}}$, and $\bar{\eta}$ denotes the electric resistivity evaluated by $\bar{\eta} = \eta_*(T_{\mathrm{e0}}^{-1.5} + L_{\mathrm{div}}/L_{\mathrm{SOL}}(T_{\mathrm{esA}}^{-1.5} + T_{\mathrm{esB}}^{-1.5}))$ and $\eta_* = \eta_\|/T_e^{-1.5}$. The equipartition energy is given by $W_{\mathrm{eeq0,A,B}} = -W_{\mathrm{ieq0,A,B}} = 1.5 n_{0,\mathrm{sA,B}}(T_{\mathrm{i0,sA,B}} - T_{\mathrm{e0,sA,B}})/\tau_{\mathrm{eq0,A,B}}$ ($\tau_{\mathrm{eq0,A,B}}$: temperature equilibration time evaluated by $T_{\mathrm{e0,sA,B}}$ and $n_{0,\mathrm{sA,B}}$). The stagnation point position is determined by $l_a/L_{\mathrm{SOL}} = (1 + \Gamma_{\mathrm{uB}}/\Gamma_{\mathrm{uA}})^{-1}$, which derived from continuous equations integrated in two SOL regions. Boundary conditions at the sheath entrances A and B are given as follows. The particle flux is given by $\Gamma_{\mathrm{sA,B}} = n_{\mathrm{sA,B}} C_{\mathrm{sA,B}}$ with $C_{\mathrm{sA,B}} = \sqrt{(T_{\mathrm{esA,B}} + 3T_{\mathrm{isA,B}})/m_i}$ based on the results from PARASOL [9]. The sheath potential is given by $\phi_{\mathrm{sA,B}} = (\beta_{\mathrm{A,B}} - \ln(1 - \sigma_{\mathrm{A,B}}\widehat{J}_{\mathrm{A,B}}))T_{\mathrm{sA,B}}/e$. The heat flux is given by $Q_{j\mathrm{sA,B}} = \gamma_j T_{j\mathrm{sA,B}}(\Gamma_{\mathrm{sA,B}} - \delta_j \sigma_{\mathrm{A,B}} J/e)$ with heat transmission coefficients $\gamma_e = 2 + e\phi_{\mathrm{sA,B}}/T_{\mathrm{esA,B}}$ and $\gamma_i = 2$–3 [4]. The time evolution of 11 equations (Eqs. (1)–(5)) with variables, n_0, n_{sA}, n_{sB}, Γ_{uA}, Γ_{uB}, T_{e0}, T_{esA}, T_{esB}, T_{i0}, T_{isA}, T_{isB}, is calculated by using the Runge–Kutta–Gill method.

3. Results

We study SOL-divertor plasmas by using the five-point model with the following parameters. The recycling coefficient η_r is an input parameter, which relates with the particle flux amplification factor R as $\eta_r = (R - 1)/R$ at the steady state. Other parameters are chosen to be typical parameters in JT-60U: total particle and electron/ion heat flows from the core to the SOL are $\Phi_{\mathrm{sep}} = 3 \times 10^{22}\ \mathrm{s}^{-1}$ and $Q_{j\mathrm{sep}} = 2$ MW, respectively. Radial diffusivities are chosen as $D_\perp = 1\ \mathrm{m}^2/\mathrm{s}$ and $\chi_{j\perp} = 2\ \mathrm{m}^2/\mathrm{s}$, respectively. Geometrical parameters are $L_{\mathrm{SOL}} = 100$ m, $L_{\mathrm{div}} = 4$ m, and the pitch of the magnetic field $\theta = 0.06$. The effective radiation factor k is chosen to be 5.

3.1. Comparison of static and dynamic features with fluid codes

Fig. 2 shows $T_{j0,\mathrm{sA,B}}$ of stable equilibria as a function of $R = 1/(1 - \eta_r)$ with fixed $\gamma_i = 2$ [4]. The SOL ion temperature T_{i0} is higher than T_{e0} for equal input powers, $Q_{\mathrm{esep}} = Q_{\mathrm{isep}}$. The ion temperature of divertor plasmas T_{is} becomes equal to T_{es} for high recycling plasmas ($R > 10$) due to the strong equipartition with high n_s and low T_{es}. When R increases up to 18 and T_{es} decreases below a critical value of $T_{es}^{\mathrm{crit}} \approx 21$ eV for $T_{e0} \approx 80$ eV, a symmetric equilibrium becomes unstable due to the thermoelectric instability and stable asymmetric equilibria appear. The SOL temperatures T_{j0} slightly increases with R for the asymmetric equilibria. Under the assumption of $T_e = T_i$, the symmetric equilibrium becomes unstable for a high critical value of $T_s^{\mathrm{crit}} \approx 29$ eV ($T_0 \approx 80$ eV) at $R = 10$ compared with Fig. 2. The equipartition energy transfer has the stabilizing effect on the thermoelectric instability.

For the model validation, we compare the results with those obtained by usual fluid codes. Fig. 3 shows the dependence of the ratio of T_{i0}/T_{e0} on a

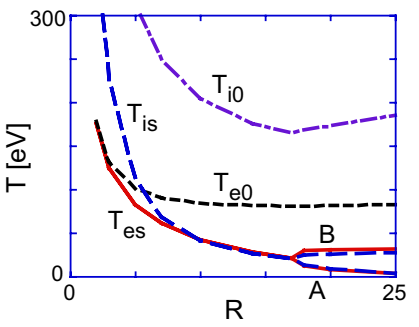

Fig. 2. Dependence of $T_{j0,\mathrm{sA,B}}$ on R. Asymmetry arises due to thermoelectric instability for $R > 18$ where divertor 'A' is low-T_s side and 'B' is high-T_s side.

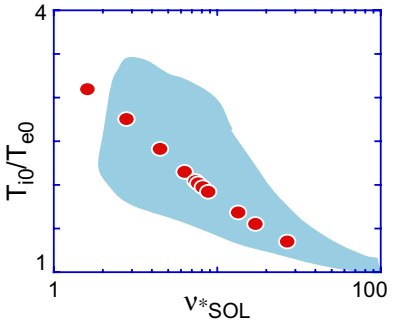

Fig. 3. Ratio of T_{i0}/T_{e0} as a function of ν^*_{SOL} where closed circles and shaded region represent results obtained by five-point model and 2D fluid code [4], respectively.

SOL collisionality defined by $\nu^*_{SOL} = 10^{-16} n_0 (L_{SOL}/2 + L_{div})/\overline{T}_0^2$, where $\overline{T}_0 = (T_{e0} + T_{i0})/2$ [eV]. The ratio of T_{i0}/T_{e0} decreases with increasing ν^*_{SOL}. The five-point model can reproduce the feature found by 2D fluid code EDGE2D and OSM [4]. When a temperature perturbation is added to an unstable symmetric equilibrium with $R = 20$ in Fig. 2, the instability leads the unstable equilibrium to a stable asymmetric one about 10 ms after the perturbation. The growth time of the thermoelectric instability is about 10 ms. These transient behavior and time scale agree well with those found in 1–1/2D fluid simulations [11].

3.2. Comparison of transient behavior with PARASOL simulation

The transient behavior of a symmetric plasma is compared with result from PARASOL [12]. Fig. 4 shows the transient behavior after an ELM crash. Calculation conditions are almost the same as in PARASOL; $L_{div} = 50$ m, $\eta_r = 0.5$, $\Phi_{sep} = 5 \times 10^{22}$ s^{-1}, $Q_{esep} = 2Q_{isep} = 0.4$ MW, and ELM sources, $\Phi_{ELM} \approx 2.5 \times 10^{24}$ s^{-1}, $Q_{eELM} \approx 2Q_{iELM} \approx 160$ MW are added during 10 μs. The value of γ_i is chosen to be 3. In Fig. 4, there are two time scales, a fast time scale of the electron transit time, $\tau_e = (L_{SOL}/2 + L_{div})/v_e \approx 15$ μs, and a slow time scale of the sound-speed transit time, $\tau_s = (L_{SOL}/2 + L_{div})/C_s \approx 550$ μs, where $v_e = \sqrt{T_{e0}/m_e}$ and C_s are evaluated by the maximum values of T_{j0}. As was pointed by Ref. [12], behaviors of T_{es}, ϕ_s and Q_{es} are on the fast time scale, those of n_s, Γ_s, T_{is} and Q_{is} are on the slow time scale. Both fast and slow behaviors obtained by the five-point model agree fairly well with those found in PARASOL. There are two discrepancies between the five-point model and the PARASOL. A shock front propagation is not taken into account (see T_{is} and Q_{is} in Fig. 4(e) and (f)). In the PARASOL results, the existence of super-thermal electrons makes Q_{es} jump on the fast time scale and the ion heat flux Q_{is} becomes a little higher than

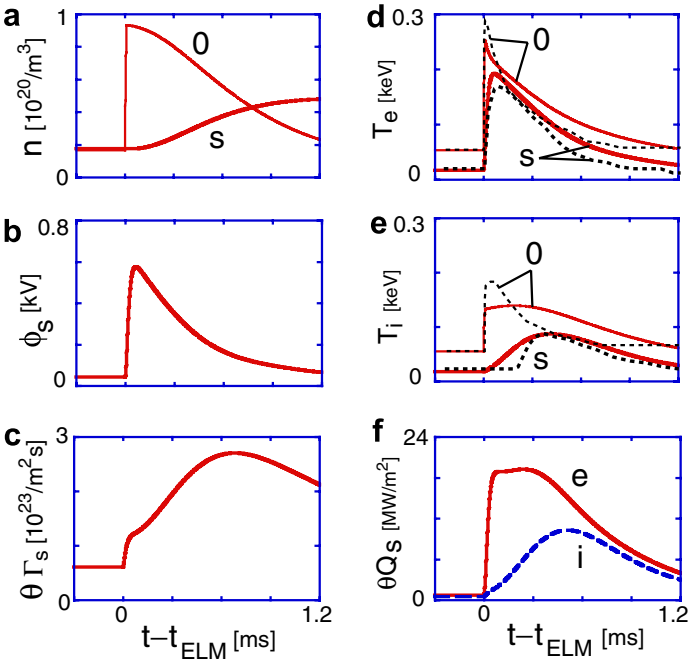

Fig. 4. Dynamic response of (a) $n_{0,s}$, (b) ϕ_s, (c) $\theta\Gamma_s$, (d) $T_{e0,s}$, (e) $T_{i0,s}$, and (f) θQ_{js}, after an ELM crash at $t = t_{ELM}$, obtained by five-point model for comparison with PARASOL [11] (shown by dotted lines in (d) and (e)).

the electron heat flux Q_{es} on the slow time scale [12]. On the other hand, in Fig. 4(f), there is no Q_{es} jump and $Q_{is} < Q_{es}$. This is due to the fixed energy transmission coefficients in the five-point model. These effects remain as future work.

3.3. ELM influence on thermoelectric instability and asymmetry

We next investigate the dynamic response of asymmetric plasmas to an ELM crash. The ELM crash is added to an asymmetric equilibrium caused by the thermoelectric instability at $R = 20$ in Fig. 2. Fig. 5 shows the time evolution after an ELM crash with $\Phi_{ELM} = 6.0 \times 10^{23}\ s^{-1}$, $Q_{eELM} = 55$ MW, $Q_{iELM} = 75$ MW during 50 μs. As shown in Fig. 5(a) and (e), the asymmetric temperature difference ($T_{esB} - T_{esA}$) grows rapidly with the increase of the SOL current about 10 μs after the ELM start. The thermoelectric instability strongly arises on the fast time scale at the value of T_{es}, which is much higher than the critical value predicted by static analyses [7]. As a result, the asymmetry of the electron heat flux is enhanced through the convective heat transport in the opposite direction of the SOL current in Fig. 5(f). After the instability enhances the electron asymmetry, the conductive heat transport mitigates the asymmetry in the last phase on the fast time scale ($t - t_{ELM} \sim 50$ μs). In this phase, because the density does not vary on the fast time scale, the pressure at the high-n_s side 'A' becomes higher than that at the low-n_s side 'B'. The upstream particle flux Γ_{uB} becomes larger than Γ_{uA} due to the pressure imbalance in Fig. 5(d). In Fig. 5(b), the T_{is} asymmetry ($T_{isA} < T_{isB}$) is enhanced due the asymmetry of n_s and Γ_u ($n_{sA} > n_{sB}$ and $\Gamma_{uA} < \Gamma_{uB}$). In Fig. 5(c), the density n_{sB} becomes higher than n_{sA} on the slow time scale. The particle flux at the sheath of the high-n_s side, Γ_{sA}, increases on the fast time scale and enhances the decrease of n_{sA}. As a result, the state of the asymmetry is reversed before ($T_{jsA} < T_{jsB}$) and after the ELM crash ($T_{jsA} > T_{jsB}$).

For the case of the ELM in the stable symmetric equilibrium at $R = 17$ in Fig. 2, the thermoelectric instability arises on the slow time scale about 1 ms after the ELM as shown in Fig. 6. This is because n_s increases and T_{es} decreases below its value before the ELM and the static unstable condition is satisfied.

4. Summary and discussion

A dynamic five-point model is developed to study the response of the SOL-divertor plasmas to an ELM crash. The five-point model is beneficial to

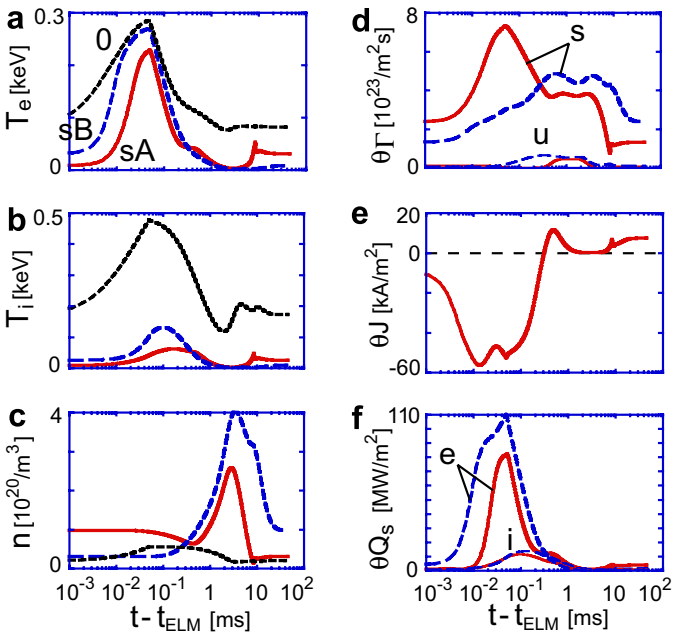

Fig. 5. Dynamic response of (a) $T_{e0,sA,B}$, (b) $T_{i0,sA,B}$, (c) $n_{0,sA,B}$, (d) $\theta\Gamma_{u,sA,B}$, (e) θJ, and (f) $\theta Q_{jsA,B}$, after an ELM crash for a stable asymmetric equilibrium with $R = 20$ shown in Fig. 2. In (a)–(d) and (f), solid, broken and dotted lines denote 'A, 'B' and '0', respectively. In (d), thick and thin lines denote 's' and 'u', respectively. In (f), thick and thin lines denote electron and ion, respectively.

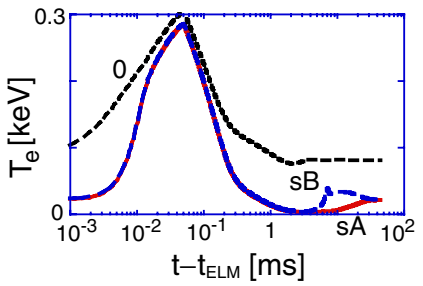

Fig. 6. Dynamic response of $T_{e0,sA,B}$ after an ELM crash for a stable symmetric equilibrium with $R = 17$ shown in Fig. 2.

wide-ranging studies of SOL-divertor physics and to coupling with the core transport code in the integrated modeling. The five-point model can reproduce static and dynamic features obtained by usual fluid codes. The dynamic behavior obtained by the five-point model agrees fairly well with that by PARASOL. The influence of the ELM crash on the thermoelectric instability and the resultant asymmetry is investigated. For asymmetric divertor plasmas before the ELM, the ELM crash transiently induces the thermoelectric instability and large SOL currents with much higher temperature than the predicted value by the static analysis. The resultant currents drive convective heat flows and enhance the asymmetry on the fast time scale of electrons. The ELM crash is found to reverse the asymmetry before and after the ELM. Even for symmetric plasmas before the ELM, the asymmetry is induced on the slow time scale of ions after an ELM crash, because the transient formation of dense and cold divertor plasmas satisfies the unstable condition obtained by the static analysis.

The reversal of the asymmetry before and after the ELM does not occur for a different set of parameters in the five-point model. The reversal is not yet seen in experiments. Thus, the parameter space in which the reversal occurs should be investigated and compared with experiments in future.

The application of the five-point model to the integrated ELM modeling is discussed. By coupling the five-point model with the core transport code, we can investigate the self-consistent transport covering core-pedestal-SOL-divertor plasmas. Study of the influence of the dynamic response of SOL-divertor plasmas on the ELM energy loss is in progress [13].

The improvement of the five-point model remains as future work. The shock front propagation and the time variation of energy transmission coefficients will be taken into account. The present five-point model cannot always reproduce all of experimental observations of the asymmetry. Effects of recycling (time variation of η_r in the model and its asymmetry ($\eta_{rA} \neq \eta_{rB}$)) and drift flows on the dynamic response of the SOL-divertor plasmas will be introduced. These model improvements allow the further validation of the model by comparing with results from experiments and other simulations.

Acknowledgements

The authors would like to thank Drs R. Hiwatari and N. Asakura for fruitful discussions. We are grateful to Dr T. Ozeki for his encouragement. This work is partly supported by a Grant-in-Aid for scientific research of Japan Society for the Promotion of Science.

References

[1] N. Asakura, M. Takechi, N. Oyama, T. Nakano, J. Nucl. Mater. 337–339 (2005) 712.
[2] R.A. Pitts et al., Nucl. Fusion 43 (2003) 1145.
[3] T.D. Rognlien, M. Shimada, J. Nucl. Mater. 313–316 (2003) 1000.
[4] P.C. Stangeby, The Plasma Boundary of Magnetic Fusion Devices, Institute of Physics Publishing, Bristol and Philadelphia, 2000.
[5] R. Hiwatari et al., J. Nucl. Mater. 337–339 (2005) 386.
[6] T. Onjun et al., Phys. Plasmas 12 (2005) 012506.
[7] N. Hayashi, T. Takizuka, A. Hatayama, M. Ogasawara, Nucl. Fusion 38 (1998) 1695.
[8] N. Hayashi, T. Takizuka, A. Hatayama, M. Ogasawara, J. Nucl. Mater. 266–269 (1999) 526.
[9] T. Takizuka, M. Hosokawa, K. Shimizu, Trans. Fusion Technol. 39 (2001) 111.
[10] W. Fundamenski, Plasma Phys. Control. Fus. 47 (2005) R163.
[11] Y. Shibata, A. Hatayama, N. Hayashi, M. Ogasawara, Contribution Plasma Phys. 40 (2000) 393.
[12] T. Takizuka, M. Hosokawa, Contribution Plasma Phys. 46 (2006) 698.
[13] N. Hayashi et al., in: Proceedings of the 21st IAEA Fusion Energy Conference, 2006, Chengdu, CD-ROM (IAEA, Vienna) file TH/4-2, 2006.